Molecular Docking and Molecular Dynamics Simulation-Based Identification of Natural Inhibitors against Druggable Human Papilloma Virus Type 16 Target

Arief Hidayatullah[1], Wira Eka Putra[2,*], Sustiprijatno[3], Diana Widiastuti[4], Wa Ode Salma[5] and Muhammad Fikri Heikal[6]

[1]Department of Biology, Faculty of Mathematics and Natural Sciences, Universitas Negeri Malang, East Java, Indonesia
[2]Biotechnology Study Program, Department of Applied Sciences, Faculty of Mathematics and Natural Sciences, Universitas Negeri Malang, East Java, Indonesia
[3]Indonesian Center for Agricultural Biotechnology and Genetic Resources Research and Development, West Java, Indonesia
[4]Department of Chemistry, Faculty of Mathematics and Natural Science, Universitas Pakuan, West Java, Indonesia
[5]Department of Nutrition, Faculty of Public Health, Halu Oleo University, Southeast Sulawesi, Indonesia
[6]Tropical Medicine International Program, Faculty of Medicine, Khon Kaen University, Khon Kaen 40002, Thailand

(*Corresponding author's e-mail: wira.putra.fmipa@um.ac.id)

Abstract

The E5 protein is the smallest known oncoprotein linked to HPV 16 cancer development. In this study, we determined the potential of asarinin and thiazolo as an inhibitor of the E5 protein through molecular dynamics. The results showed that the binding site is unstable because of its hydrophobic nature and small size, causing considerable changes in the binding site for each of the 3 drugs examined. Except for asarinin, which still interacts with the first hydrophobic domain, they preserved their capacity to prevent endosomal acidification, hyper amplification of the EGFR pathway and contact with BAP31. It may inhibit E5-MHC I interaction. Thiazolo[3,2-a]benzymidazole-3(2H)-one,2-(2-fluorobenzylideno)-7,8-dimethyl (thiazolo) is expected to form more stable protein-ligand complexes than the other 2. However, the SASA, hydrogen bond and DCCM plots show that both compounds are equivalent to HPV 16 E5 protein.

Keywords: E5 protein, HPV16, Molecular dynamics, Ligand conformation, Ligand movement

Introduction

Human papillomaviruses (HPVs) are small double-stranded non-enveloped DNA viruses that infect the skin and mucosa epithelium [1-3]. At least 202 HPVs have been identified, although studies indicate that the actual number is much higher [4-6]. It is generally classified into 2 major groups: The low-risk HPV, which commonly cause benign epithelial lesion with low mortality prevalence and high-risk HPV, which cause urogenital and head and neck cancer with high mortality prevalence and accumulation [7,8].

HPV is linked to 5 % of all cancers globally, including cervical cancer and head and neck squamous cell carcinoma (HNSCC), and the proportion of HPV-associated malignancy has been rising. A subset of HPVs are carcinogenic, and HPV16 is identified in about 60 % of cervical cancer cases globally [9,10]. Cervical cancer is the second most frequently occurring form of cancer in Indonesia and the second most frequently occurring type in females aged 15 to 44 [11,12]. Infections of high-risk HPV are commonly asymptomatic. However, it could be detected during screening by looking for precancerous lesions [13]. The main risk for high-risk genital HPV infection are being sexually active, having a non-monogamous sexual partner, being sexually active at an earlier age, and having a higher number of sexual partners [14,15]. The efforts to prevent high-risk HPV infections may take 1 of 2 directions: A preventive strategy based on vaccination or a curative approach based on treatment [16,17]. Vaccination is the most feasible preventive option that provides maximum protection against high-risk HPV infections. At least more than 80 countries have introduced nationwide HPV vaccination programs [18]. The most commonly used HPV

vaccines are Gardasil, Gardasil 9 and Cervarix [19]. Combined with safer or lower-risk sexual activity, it significantly reduced the chance of getting infected by high-risk HPV [20]. Meanwhile, despite decades of research, there is currently no effective treatment for a persistent HPV infection. Some therapies do not thoroughly remove HPV DNA, leaving a 40 % risk of infection recurrence [21].

Although no effective HPV inhibitors have been developed, several compounds and targets have been analyzed. Most research on HPV-related cancer has focused on the oncoproteins-proteins encoded by HPV's oncogenes that are highly involved in the synthesis and regulation of tumor-associated proteins [22,23] -particularly E6 and E7. Due to their well-characterized activities and pathways, these proteins are critical oncoproteins that differentiate high-risk from low-risk variations [5,24-26]. However, another essential oncoprotein for the HR type of HPV is the E5 protein, an 83 amino acid long hydrophobic transmembrane protein that interacts with various cellular proteins biologically critical during cell transformation. HPV 16 E5 is classified as an oncoprotein due to its ability to induce anchorage-independent growth in murine fibroblasts and human keratinocytes [10]. By inhibiting the tumor suppressors, p21 and p27 decreases the expression of MHC I and BAP31 in the ER and increase infection cell entrance into the S-phase [27-29]. We predict asarinin, and thiazolo in our recent molecular docking research as potent E5 protein inhibitors is mainly due to their docking affinity, stability and predicted binding site. They are expected to interact with 3 critical regions of the E5 protein, specifically the first hydrophobic domain, the third hydrophobic domain and the C-terminus, disrupting the E5 protein's interaction with the heavy chain of MHC I, inhibiting endosomal acidification mediated by v-ATPase, and decreasing the rate of EFG-receptor recycling to the plasma membrane, respectively [10,27,30-33].

Rimantadine is an antiviral medication classified as a viroporin blocker. This orally available drug is most commonly used to treat influenza A virus infection. It interferes with the virus's uncoating process, inhibiting the ion channel formed by the M2 protein that crosses the viral membrane, and reducing viral replication [34]. Combining 5 μM rimantadine and 0.1 μM zanamivir significantly reduced H1N1 virus generation in MDCK cells by 90 - 100 % [35]. Rimantadine reduced the p7 protein's activity against the Hepatitis C virus (HCV) in Huh7 cell culture with an IC50 value of 40 μM [36]. Rimantadine's *in vitro* repurposing as an E5 inhibitor inhibited the target protein with a 100 μM IC50. Prior research predicted that inhibiting E5's voltage gating motifs would inhibit the activation of mitogenic signaling in keratinocytes [37]. We perform further research in this work utilizing various molecular dynamic characteristics to evaluate the potential of asarinin and thiazolo as an inhibitor of the E5 protein.

Materials and methods

Data retrieval and pre-docking screening

The HPV16 E5 amino acid sequence was collected from UniProt under the accession number P06927. The protein's 3-dimensional structure was simulated using the I-TASSER website (https://zhanglab.dcmb.med.umich.edu/I-TASSER/). The 3D model was picked based on its C- and TM-score values rank. We assessed the modelled structure using SWISS-MODEL (https://swissmodel.expasy.org/assess). The Ramachandran favored percentage was 57.14 % with MolProbity score of 3.73. The final file format for the target protein is .pdb. We evaluated asarinin and thiazolo, the top 2 ligands with the lowest binding affinity scores, as well as vorinostat (CID:5311) as a positive control. All compounds were provided in .sdf format.

Molecular docking process

AutoDock Vina is used for docking, integrated with PyRx (https://pyrx.sourceforge.io). Before the docking procedure, we convert protein target molecule and ligands into .pdbqt format, required by Autodock Vina. We used the target protein's whole structure for this blind docking procedure. The molecular coverage area, which include whole structure of the protein, is 39.3567×40.9481×35.1306 Å, and the center coordinates are 56.3238×40.9481×35.1306 Å. The main factors in docking are the molecule's affinity in kcal/mol, where the binding site is, and how the protein and ligands interact.
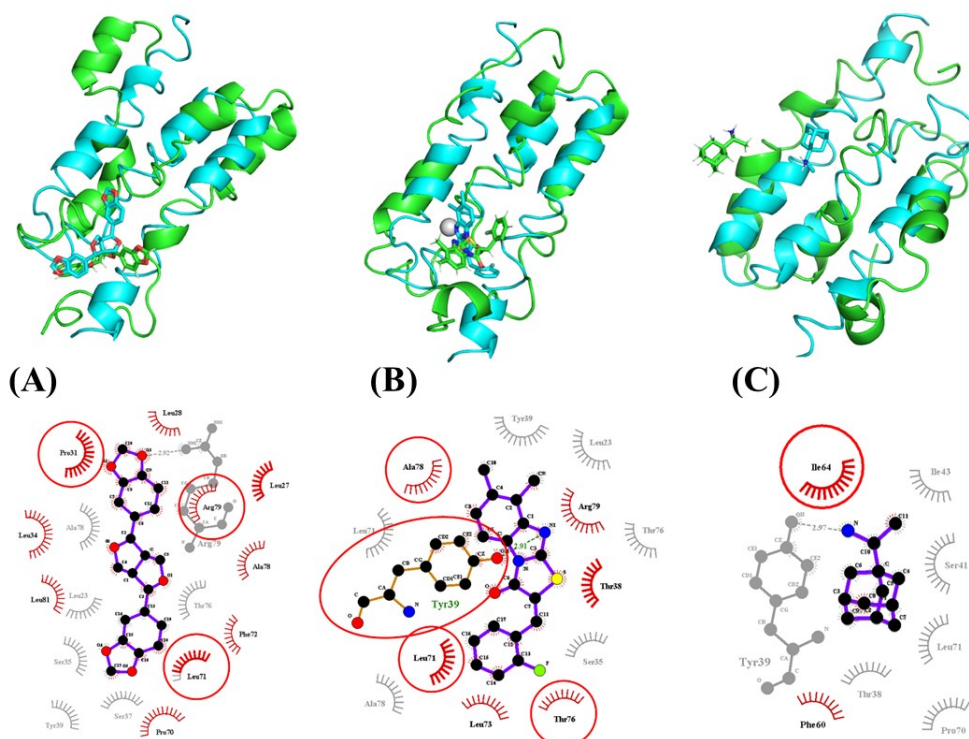
Molecular dynamics simulation

During simulating molecular dynamics against the E5 protein, ligands with the lowest scores for binding affinity were chosen. Under physiological conditions 37 °C, 1 atm, pH 7.4 and 0.9 % salinity, the protein and ligand complex structures were built for 1,000 picosecond simulations. The md run macro program was used to do the molecular dynamics simulation, and the md analyze, and md analyeres macro programs were used to analyze the molecular dynamics data through yasara.

Results and discussion

The alignment of the 3 protein-ligand complexes in 3 dimensions using a cycle value of 5.0 and a cutoff value of 2.0 revealed that they deviate by more than 5 Å. However, the lowest deviation was seen in the E5-thiazolo complex, which had an RMSD alignment value of 5.575 Å. The E5-asarinin complex exhibited the highest alignment, with a score of 7.060 Å. Visual inspection of the binding site using 3D visualization revealed that asarinin and thiazolo did not exhibit a substantial shift in position. However, when rimantadine was used as a control, substantial alterations in the binding site were observed.

Table 1 Binding site residues comparison before and after molecular dynamics simulation.

| Compounds (CID)	Sources (organ)	Pre-molecular dynamics simulation		Post-molecular dynamics simulation	
		Amino acid residue	Interactions (Å)	Amino acid residue	Interactions (Å)
Asarinin (11869417)	*Zanthoxylum spp* (bark)	Thr76	Hydrophobic contact	Arg79	Hydrophobic contact
		Leu71		Leu28	
		Ser37		Ala78	
		Tyr39		Leu81	
		Ser35		Leu71	
		Leu23		Pro70	
		Ala78		Phe72	
		Pro31		Pro31	
		Arg79	Hydrophobic contact Hydrogen bond (2.92)	Leu34	
				Leu27	
Thiazolo (1823738)	*Myristica fragrans* (seeds)	Tyr39	Hydrophobic contact	Ala78	Hydrophobic contact
		Leu23		Leu71	
		Thr76		Leu73	
		Ser35		Thr76	
		Ala78		Thr38	
				Arg79	
		Leu71		Tyr39	Hydrophobic contact Hydrogen bond (2.91)
Rimantadine (5071)	Drug control	Pro70	Hydrophobic contact	Ile64	Hydrophobic contact
		Thr38		Phe60	
		Leu71			
		Ile64			
		Ser41			
		Ile43			
		Tyr39	Hydrophobic contact Hydrogen bond (2.97)		

Figure 1 The 3D and 2D structure visualization of binding HPV16 E5 protein and (A) asarinin, (B) thiazolo, (C) rimantadine. The cyan structures in 3D visualization indicate the protein-ligand complex before MD simulation, while the green structures are after MD simulation. The colored diagram in 2D indicates protein-ligand complex after MD, while the greyscale diagram indicates protein-ligand complex before MD.

The outcomes of the 2-dimensional visualization (**Table 1** and **Figure 1**) are comparable to those of the 3-dimensional visualization. Rimantadine, used as a control, exhibited the most substantial alteration in the binding site, with a roughly 70 % decrease in interaction with binding site residues compared to the pre-MD state. Only 2 residues, notably Ile64 and Phe60, interact with rimantadine through hydrophobic interactions. The 2D visualization findings revealed that the asarinin binding site shifted throughout the simulation period, as shown by just 4 of the 9 conserved residues. Asarinin's interaction with 1 other deposition increased from 9 to 10 residues. Additionally, it lost hydrogen bonds with the binding site residues, rendering all interactions between asarinin and its binding site are through hydrophobic contact. The 2-dimensional visualization revealed that thiazolo also underwent binding site shift, as shown by substituting 2 interacting residues and inserting 1 additional interacting residue. Post-molecular dynamics simulations revealed that thiazolo established a second hydrogen bond with Tyr39. Based on these results, asarinin still interacts with residues in the first hydrophobic domain, third hydrophobic domain and C-terminal region, but the post-MD results show that all residues that interact with asarinin are critical residues in each region. Thiazolo losing its interaction with the residue of the first hydrophobic domain, so it only interacts with the third hydrophobic domain and C-terminal region. Rimantadine control practically only interacts with residues in the third hydrophobic domain instead of the second and third hydrophobic domain before MD simulation.

The 2 visualization results demonstrate that the 3 ligands' binding sites shifted following MD simulation. Because asarinin's binding site shifting in post-MD simulation, positioned in between the first, third hydrophobic domains and the extreme C-terminal domain, asarinin could theoretically disrupt the E5 protein's interaction with the heavy chain of MHC I by interacting primarily with Pro31, thereby decreasing endosomal acidification and the rate of EGFR recycling, and inhibiting the interaction of E5 protein with BAP31, respectively [27,38-41]. However, asarinin's binding site did not exhibit substantial visual changes than the pre-MD state, suggesting that the binding location was optimum for asarinin, particularly after passing 700 ps. Between 150 and 700 ps, fluctuations in ligand movement are believed to be driven by its binding pocket showing some flexibility before stabilizing at 700 ps [42]. Meanwhile, asarinin's

conformational variation was caused by its attempt to maintain contact with the changing binding pocket on the E5 protein [43]. However, asarinin's conformational plot pattern suggested it had not yet achieved equilibrium [44].

After 700 ps, the ligand mobility plot exhibits comparable findings to the 2D and 3D representations. Asarinin has the most significant mean value (9.225 ± 2.618 Å), indicating rapid movement in the time range of 100 to 700 ps with a maximum peak at 13.813 Å and then rapidly decreasing to around 7 Å before finally stabilizing about 100 ps before the simulation period ended, just below thiazolo. Rimantadine has the lowest average movement (5.622 ± 2.278 Å), and it is reasonably steady around 5 Å, but exhibits a dramatic and rapid rise in RMSD movement value shortly after 900 ps, reaching a maximum of 13.365 Å. The ligand with the most stable movement in this simulation is thiazolo, as indicated by the RMSD plot pattern, which has the most stable plot in comparison to other ligands, despite it did not have the lowest mean value of movement, but it has lowest standard deviation value among others (7.318 ± 1.252 Å).
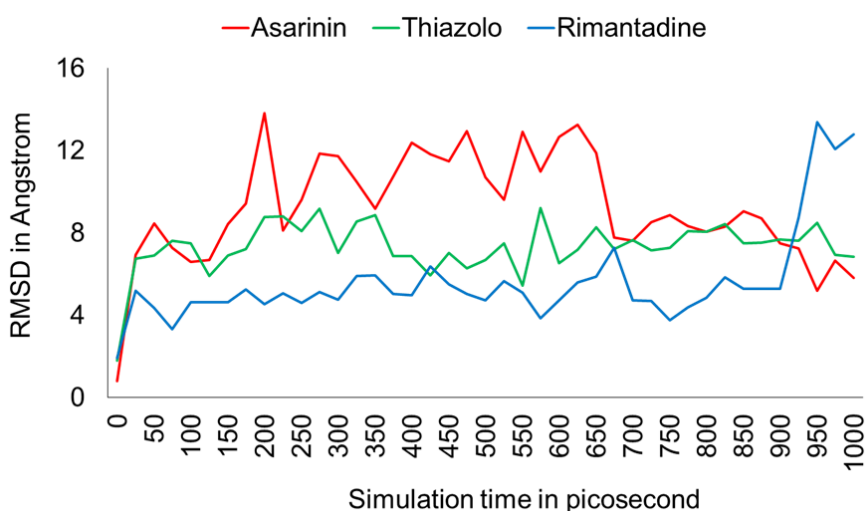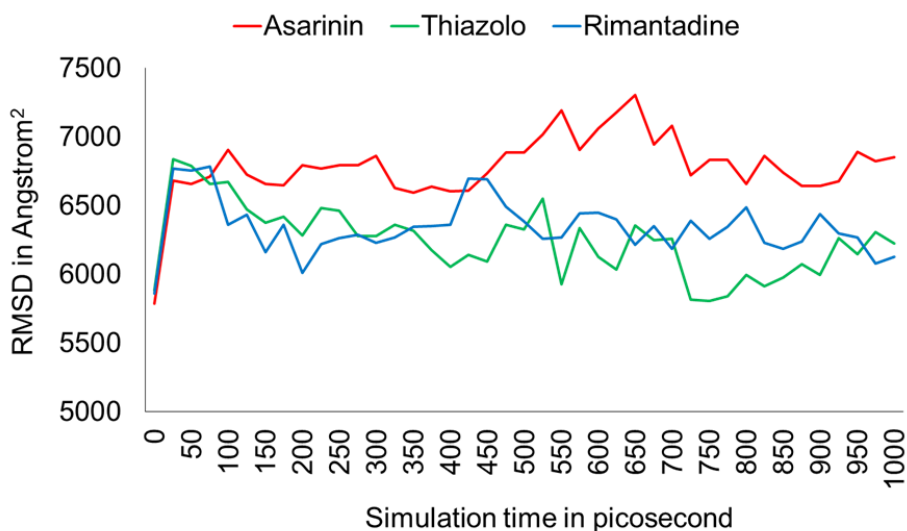

Figure 2 Ligand movement plot for asarinin (red line), thiazolo (green line) and rimantadine (blue line) over a 1,000 picosecond of simulation.

Rimantadine is the only ligand with no significant conformational fluctuations and the mean conformational deviation less than 1 Å (0.796 ± 0.144 Å). While both asarinin and thiazolo exhibited significant conformational fluctuations. Simulation results indicated that asarinin exhibited slightly more conformational changes than thiazolo. Asarinin's standard deviation (0.454 Å) is marginally higher than thiazolo (0.398 Å). Additionally, the plot results indicated that asarinin fluctuated from 50 ps to the end of the simulation period. In contrast, thiazolo also fluctuated but stabilized at around 2 Å between 200 - 400 ps and 700 - 950 ps, before finally dropping below 2 Å at the end of the simulation.

In general, thiazolo exhibits relatively consistent movement and conformation plots when compared to the other ligands examined, as indicated by a relatively low standard deviation value [45,46]. When the binding pocket of the compounds was visually compared before and after MD, no significant alterations were seen. The relatively steady movement and conformation plot showed that the binding site was optimized and that conformational changes occurred due to adjusting the conformation with its binding site [42,43,47]. Nevertheless, thiazolo loses its interaction with the first hydrophobic domain and retains it with the third hydrophobic domain and the C-terminal domain, reducing its ability to disrupt the E5 protein's interaction with the heavy chain of MHC I but retaining its ability to inhibit endosomal acidification, the EGFR pathway hyperamplification, and inhibit the interaction of E5 protein with BAP31 which reducing infected cells' proliferation ability and the virion assembly process [27,38-41].
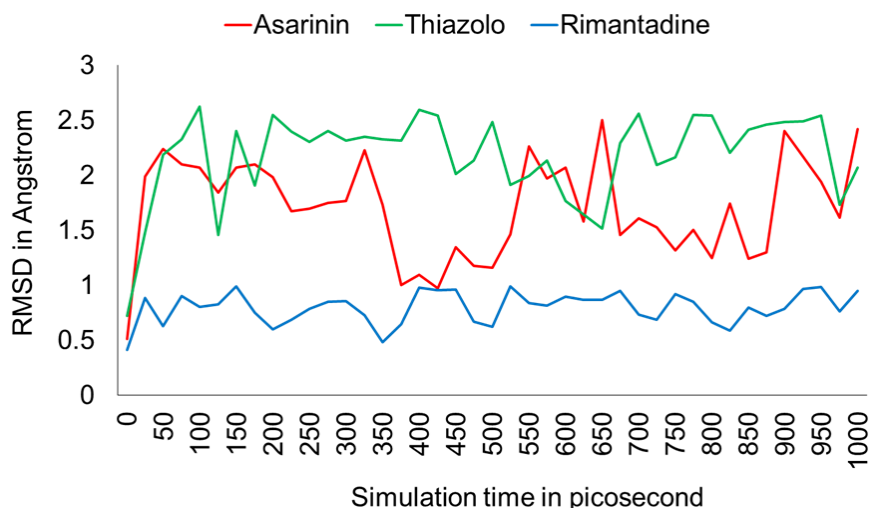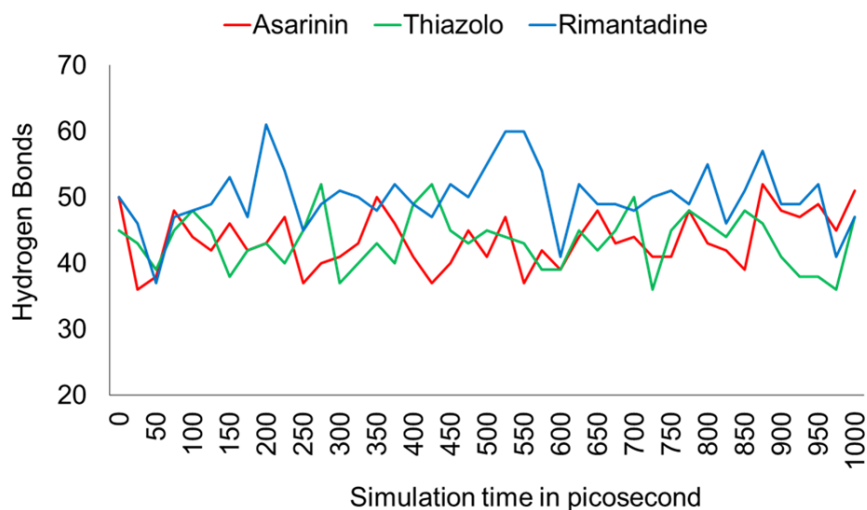
Figure 3 Ligand conformation plot for asarinin (red line), thiazolo (green line) and rimantadine (blue line) over a 1,000 picosecond of simulation.
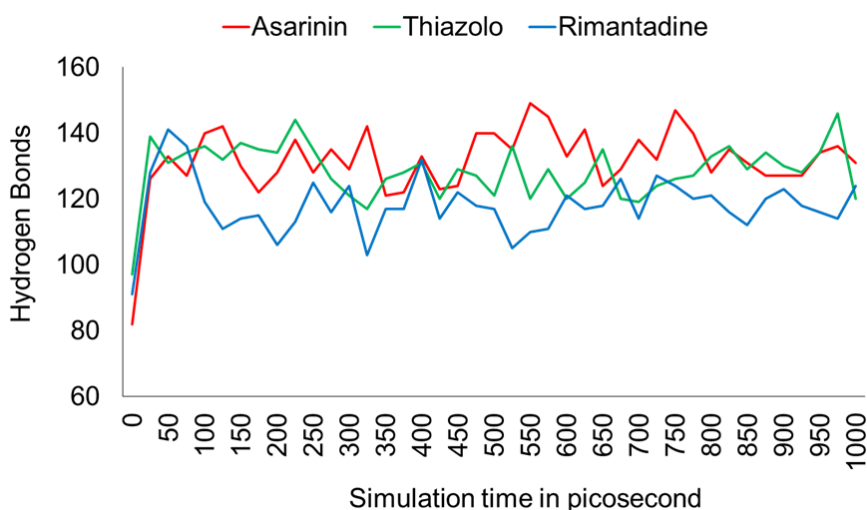

Figure 4 Solvent accessible surface area for asarinin (red line), thiazolo (green line) and rimantadine (blue line) complexes over a 1,000 picosecond of simulation.

The most drastic positional shift was experienced by rimantadine, which is known as an anti-viroporin drug, where it expelled from its binding cavity compared to the pre-MD simulation results. However, post-MD rimantadine is predicted to still interact with Ile64, which is thought to be an essential residue that acts as a voltage gating motif that inhibits the diffusion of specific critical ions, although the intricacies of the voltage gating motif's function on the HPV16 E5 protein remain mostly unclear [30,48]. The lack of interaction between rimantadine and Ser41 after the simulation is believed to reduce the possibility of inhibiting mitogenic signaling activation for this specific protein in keratinocytes, but these results still need to be explored further through *in vitro* studies [10,37,48]. The abrupt ligand movement of rimantadine towards different binding sites in the last 100 ps of simulation indicates that the initial binding site of rimantadine may not be optimum owing to the conformational dynamics of the E5 protein throughout the simulated process [42,49]. Rimantadine's stable conformation ligand is believed to be owing to its simple structure as a cyclic amine, which provides little flexibility.

Figure 5 Intramolecular hydrogen bonds in the solute for asarinin (red line), thiazolo (green line) and rimantadine (blue line) complexes over a 1,000 picosecond of simulation.

Figure 6 Hydrogen bonds between solute and solvent plot for asarinin (red line), thiazolo (green line) and rimantadine (blue line) complexes over a 1,000 picosecond of simulation.

In the 1,000 ps simulation, the solvent-accessible surface area (SASA) graph demonstrates a substantial change after 100 ps. The SASA values for the E5-asarinin complex were consistently greater than those for the 2 protein complexes. Meanwhile, the E5-thiazolo and E5-rimantadine complexes vary around 6,000 Å^2. The E5-rimantadine complex, on the other hand, exhibits a more stable graph than the 2 active molecules. However, none of the 3 protein complexes demonstrated a significant spike in SASA levels in a short period.

The SASA value fluctuated significantly during the simulation, indicating that the protein-ligand complex expanded throughout the simulation period. This expansion occurs due to the partial unfolding of the target protein, which alters the protein region accessible to solvent molecules [50-52]. Despite the fluctuations, none of the 3 protein-ligand complexes in the 1,000 ps timeframe experienced a sudden rapid change in their SASA value, indicating that the 3 protein-ligand complexes are compact enough to avoid collapsing during the simulation due to the sudden unfolding process, exposing the hydrophobic core of the protein complexes to the solvent and causing damage [53,54].

During the simulation, the intramolecular hydrogen bond plot revealed that the 3 protein complexes underwent substantial variations in size compared to the protein complexes. The most substantial hydrogen bond instability was seen in the E5-rimantadine complex. The intramolecular hydrogen bonds between the

complexes E5-asarinin and E5-thiazolo varied between 40 and 50, and both equally fluctuated. Meanwhile, the protein-solvent hydrogen bond plot demonstrates that despite the fluctuation of the 3 protein-ligand complexes, the E5-thiazolo complex has the most stable graph compared to the other protein-ligand complexes. The E5-rimantadine complex seemed to be subjected to the most substantial changes. However, both hydrogen bond graphs do not exhibit a sharp rise or drop in value throughout the simulation.

Hydrogen bond analysis revealed substantial fluctuations in both parameters, indicating that the 3 protein-ligand complexes underwent continuous movement to reach equilibrium during the simulation period [55,56]. The plot values that seem to fluctuate significantly are believed to be caused by the highly hydrophobic nature of the E5 protein and its small size. The oscillating intramolecular bond is caused by the highly hydrophobic protein complex attempting to retain its folded conformation in a water solvent to avoid a rapidly unfolded phenomenon that causes protein denaturation [57-59]. The absence of a rapid and sustained decrease in intramolecular hydrogen bonding indicated that the 3 protein complexes maintained their conformation throughout the simulation period. It correlates with the protein-solvent hydrogen bond plot, which, although fluctuating, does not exhibit a sudden and sustained spike of protein-solvent hydrogen bonds, as donor and acceptor atoms that had previously established intramolecular hydrogen bonds are exposed and form hydrogen bonds with the water [57-59].

Asarinin – E5   Thiazolo – E5   Rimantadine – E5
Complex   Complex   Complex
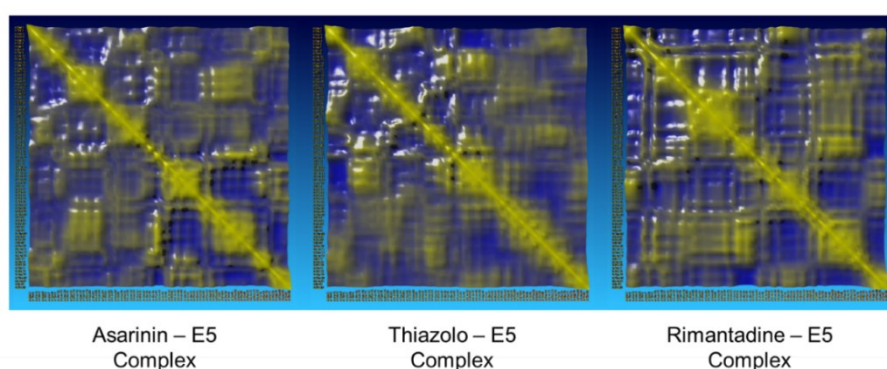
Figure 7 Dynamic cross-correlation matrix for each protein complex. Yellow represents correlated motions and blue represents anticorrelated motions.

The DCCM illustrates movements between individual residues that are considerably correlated in yellow and highly anticorrelated motions in blue [60-62] (**Figure 8**). It is shown that the E5-rimantadine complex enhanced both correlated and anticorrelated motion, implying higher fluctuation and interaction between residues within the complex. Rimantadine's binding site in the third hydrophobic domain moves in lockstep with the -helix in the first hydrophobic domain and the N-terminal of the α-helix in the second hydrophobic domain. Additionally, a strongly correlated motion was seen between residues 20 and 42, and activity of the N-terminal α-helix residue in the first hydrophobic domain (AA 8 and 10) resulted in a highly correlated movement from the first hydrophobic domain to the N-terminal of the second hydrophobic domain. A significantly anticorrelated motion was seen between the C-terminal of the second α-helix and the N-terminal of the third α-helix.

Except for the second α-helix, the E5-asarinin complex exhibits a pattern of highly correlated motion comparable to that of the E5-rimantadine complex in the first, second and third hydrophobic domains. A similar pattern was seen in the third hydrophobic domain; however, in the E5-asarinin complex, the Ser41 residue exhibited a strongly correlated motion with residues 60 - 71. Similar to the E5-rimantadine complex, a significantly anticorrelated movement was seen between the C-terminal of the second α-helix and the N-terminal of the third α-helix. However, previous studies mentioned that rimantadine act as anti-viroporin by blocking the E5 oligomer's lumen through interaction with Ser37 and Ser4, inhibiting mitogenic signaling activation in keratinocytes [10,37,48].

The E5-thiazolo complex displays a motion pattern virtually identical to the E5-asarinin complex but with a lower value. Only the first hydrophobic domain and the second N-terminal of the α-helix exhibit highly correlated mobility. The DCCM analysis demonstrates that all protein-ligand complexes display comparable patterns of correlated motions. The majority of correlated motion occurred on the α-helixes, particularly the first α-helix, the N-terminal of the α-helix of the second hydrophobic domain and the third α-helix. The E5-rimantadine complex was the most flexible, whereas the E5-thiazolo complex was the least

flexible. Correlation increased due to increased interaction with the E5-rimantadine system, implying that the system as a whole had grown more elastic compared to 2 other complexes [63,64].

Conclusions

The E5 protein is the smallest known oncoprotein related to cancer formation due to HPV 16 infection. Due to its extremely hydrophobic nature and diminutive size, the binding site is unstable, resulting in a significant change in the binding site for each of the 3 compounds studied as they seek to maintain contact with the shifting binding pocket on the E5 protein. After the simulation, the majority of them concentrated in the third hydrophobic domain and the C-terminal domain, where they retained their ability to inhibit endosomal acidification, hyperamplification of the EGFR pathway, and interaction with BAP31, except for asarinin, which still interacts with the first hydrophobic domain. It may block the interaction of E5 with MHC I. The SASA, hydrogen bond, and DCCM plots, on the other hand, indicate that both compounds are comparable against HPV 16 E5 protein. Due to its differing molecular dynamic characteristics, thiazolo is projected to create more stable protein-ligand complexes than the others.

Acknowledgements

References

[1] M Tao, M Kruhlak, S Xia, E Androphy and ZM Zheng. Signals that dictate nuclear localization of human papillomavirus type 16 oncoprotein E6 in living cells. *J. Virol.* 2003; **77**, 13232-47.

[2] M Forcier and N Musacchio. An overview of human papillomavirus infection for the dermatologist: Disease, diagnosis, management, and prevention. *Dermatol. Ther.* 2010; **23**, 458-76.

[3] W Bonnez. *Chapter 26 - human papillomavirus. In*: ADT Barrett and LR Stanberry (Eds.). Vaccines for biodefense and emerging and neglected diseases. Academic Press, London, 2009, p. 469-96.

[4] D Bzhalava, P Guan, S Franceschi, J Dillner and G Clifford. A systematic review of the prevalence of mucosal and cutaneous human papillomavirus types. *Virology* 2013; **445**, 224-31.

[5] SV Graham. The human papillomavirus replication cycle, and its links to cancer progression: A comprehensive review. *Clin. Sci.* 2017; **131**, 2201-21.

[6] F Cobo. *Introduction and epidemiological data. In*: F Cobo (Ed.). Human papillomavirus infections. Woodhead Publishing, Cambridge, 2012, p. 1-14.

[7] N Egawa and J Doorbar. The low-risk papillomaviruses. *Virus Res.* 2017; **231**, 119-27.

[8] K Kobayashi, K Hisamatsu, N Suzui, A Hara, H Tomita and T Miyazaki. A review of HPV-related head and neck cancer. *J. Clin. Med.* 2018; **7**, 241.

[9] S Miyauchi, PD Sanders, K Guram, SS Kim, F Paolini, A Venuti, EEW Cohen, JS Gutkind, JA Califano and AB Sharabi. HPV16 E5 mediates resistance to PD-L1 blockade and can be targeted with rimantadine in head and neck cancer. *Canc. Res.* 2020; **80**, 732-46.

[10] LF Wetherill, KK Holmes, M Verow, M Müller, G Howell, M Harris, C Fishwick, N Stonehouse, R Foster, GE Blair, S Griffin and A Macdonald. High-risk human papillomavirus E5 oncoprotein displays channel-forming activity sensitive to small-molecule inhibitors. *J. Virol.* 2012; **86**, 5341-51.

[11] ADR Nurcahyanti. Cervical cancer: The case in Indonesia and natural product based therapy. *J. Canc. Biol. Res.* 2016; **4**, 1078.

[12] EJ Domingo, R Noviani, MR Noor, CA Ngelangel, KK Limpaphayom, TV Thuan, KS Louie and MA Quinng. Epidemiology and prevention of cervical cancer in Indonesia, Malaysia, the Philippines, Thailand and Vietnam. *Vaccine* 2008; **26**, M71-9.

[13] PV Chin-Hong and GE Reid. Human papillomavirus infection in solid organ transplant recipients: Guidelines from the American society of transplantation infectious diseases community of practice. *Clin. Transplant.* 2019; **33**, e13590.

[14] C Chelimo, TA Wouldes, LD Cameron and JM Elwood. Risk factors for and prevention of human papillomaviruses (HPV), genital warts and cervical cancer. *J. Infect.* 2013; **66**, 207-17.

[15] M Yamaguchi. Risk factors for HPV infection and high-grade cervical disease in sexually active Japanese women. *Sci. Rep.* 2021; **11**, 2898.

[16] WK Huh, EA Joura, AR Giuliano, OE Iversen, RP Andrade, KA Ault, D Bartholomew, RM Cestero, EN Fedrizzi, AL Hirschberg, MH Mayrand, AM Ruiz-Sternberg, JT Stapleton, DJ Wiley, A Ferenczy, R Kurman, BM Ronnett, MH Stoler, J Cuzick, …, A Luxembourg. Final efficacy, immunogenicity,

and safety analyses of a nine-valent human papillomavirus vaccine in women aged 16-26 years: A randomised, double-blind trial. *Lancet* 2017; **390**, 2143-59.

[17] M El-Zein, L Richardson and EL Franco. Cervical cancer screening of HPV vaccinated populations: Cytology, molecular testing, both or none. *J. Clin. Virol.* 2016; **76**, S62-8.

[18] KE Gallagher, DS LaMontagne and D Watson-Jones. Status of HPV vaccine introduction and barriers to country uptake. *Vaccine* 2018; **36**, 4761-7.

[19] DM Harper and LR DeMars. HPV vaccines - a review of the first decade. *Gynecol. Oncol.* 2017; **146**, 196-204.

[20] E Kumakech, S Andersson, H Wabinga, C Musubika, S Kirimunda and V Berggren. Cervical cancer risk perceptions, sexual risk behaviors and sexually transmitted infections among bivalent human papillomavirus vaccinated and non-vaccinated young women in Uganda - 5 year follow up study. *BMC Wom. Health* 2017; **17**, 40.

[21] M Toots, M Ustav, A Männik, K Mumm, K Tämm, T Tamm, E Ustav and M Ustav. Identification of several high-risk HPV inhibitors and drug targets with a novel high-throughput screening assay. *Plos Pathogens* 2017; **13**, e1006168.

[22] J Durzynska, K Lesniewicz and E Poreba. Human papillomaviruses in epigenetic regulations. *Mutat. Res. Rev. Mutat. Res.* 2017; **772**, 36-50.

[23] DA Hareża, JR Wilczyński and E Paradowska. Human papillomaviruses as infectious agents in gynecological cancers. Oncogenic properties of viral proteins. *Int. J. Mol. Sci.* 2022; **23**, 1818.

[24] A Pal and R Kundu. Human papillomavirus E6 and E7: The cervical cancer hallmarks and targets for therapy. *Front. Microbiol.* 2020; **10**, 3116.

[25] NSL Yeo-Teh, Y Ito and S Jha. High-risk human papillomaviral oncogenes E6 and E7 target key cellular pathways to achieve oncogenesis. *Int. J. Mol. Sci.* 2018; **19**, 1706.

[26] J Doorbar, W Quint, L Banks, IG Bravo, M Stoler, TR Broker and MA Stanley. The biology and life-cycle of human papillomaviruses. *Vaccine* 2012; **30**, F55-70.

[27] A Venuti, F Paolini, L Nasir, A Corteggio, S Roperto, MS Campo and G Borzacchiello. Papillomavirus E5: The smallest oncoprotein with many functions. *Mol. Canc.* 2011; **10**, 140.

[28] D DiMaio and L Petti. The E5 proteins. *Virology* 2013; **445**, 99-114.

[29] M Gruener, IG Bravo, F Momburg, A Alonso and P Tomakidi. The E5 protein of the human papillomavirus type 16 down-regulates HLA-I surface expression in calnexin-expressing but not in calnexin-deficient cells. *Virol. J.* 2007; **4**, 116.

[30] R Nath, CA Mant, B Kell, J Cason and JM Bible. Analyses of variant human papillomavirus type-16 E5 proteins for their ability to induce mitogenesis of murine fibroblasts. *Canc. Cell Int.* 2006; **6**, 19.

[31] MI Rodríguez, ME Finbow and A Alonso. Binding of human papillomavirus 16 E5 to the 16 kDa subunit c (proteolipid) of the vacuolar H + −ATPase can be dissociated from the E5-mediated epidermal growth factor receptor overactivation. *Oncogene* 2000; **19**, 3727-32.

[32] GH Ashrafi, M Haghshenas, B Marchetti and MS Campo. E5 protein of human papillomavirus 16 downregulates HLA class I and interacts with the heavy chain via its first hydrophobic domain. *Int. J. Canc.* 2006; **119**, 2105-12.

[33] JA Regan and LA Laimins. Bap31 is a novel target of the human papillomavirus E5 protein. *J. Virol.* 2008; **82**, 10042-51.

[34] D Neofytos, C El-Beyrouty and JA DeSimone. *Chapter 12 - pharmacobiology of infections. In*: SA Waldman and A Terzic (Eds.). Pharmacology and therapeutics: Principles to practice. W. B. Saunders, Philadelphia, 2009, p. 173-91.

[35] EA Govorkova, HB Fang, M Tan and RG Webster. Neuraminidase inhibitor-rimantadine combinations exert additive and synergistic anti-influenza virus effects in MDCK cells. *Antimicrob. Agents Chemother.* 2004; **48**, 4855-63.

[36] TL Foster, GS Thompson, AP Kalverda, J Kankanala, M Bentham, LF Wetherill, J Thompson, AM Barker, D Clarke, M Noerenberg, AR Pearson, DJ Rowlands, SW Homans, M Harris, R Foster and S Griffin . Structure-guided design affirms inhibitors of hepatitis C virus p7 as a viable class of antivirals targeting virion release. *Hepatology* 2014; **59**, 408-22.

[37] LF Wetherill, CW Wasson, G Swinscoe, D Kealy, R Foster, S Griffin and A Macdonald. Alkyl-imino sugars inhibit the pro-oncogenic ion channel function of human papillomavirus (HPV) E5. *Antivir. Res.* 2018; **158**, 113-21.

[38] MS Campo, SV Graham, MS Cortese, GH Ashrafi, EH Araibi, ES Dornan, K Miners, C Nunes and S Man. HPV-16 E5 down-regulates expression of surface HLA class I and reduces recognition by CD8 T cells. *Virology* 2010; **407**, 137-42.

[39] F Abe, NV Prooyen, JJ Ladasky and M Edidin. Interaction of Bap31 and MHC class I molecules and their traffic out of the endoplasmic reticulum. *J. Immunol.* 2009; **182**, 4776-83.

[40] M Müller, EL Prescott, CW Wasson and A Macdonald. Human papillomavirus E5 oncoprotein: Function and potential target for antiviral therapeutics. *Future Virol.* 2015; **10**, 27-39.

[41] KK Halavaty, J Regan, K Mehta and L Laimins. Human papillomavirus E5 oncoproteins bind the A4 endoplasmic reticulum protein to regulatze proliferative ability upon differentiation. *Virology* 2014; **452-453**, 223-30.

[42] HTT Lai, A Giorgetti, G Rossetti, TT Nguyen, P Carloni and A Kranjc. The interplay of cholesterol and ligand binding in hTSPO from classical molecular dynamics simulations. *Molecules* 2021; **26**, 1250.

[43] A Gutteridge and J Thornton. Conformational change in substrate binding, catalysis and product release: An open and shut case? *FEBS Lett.* 2004; **567**, 67-73.

[44] EC Hulme and MA Trevethick. Ligand binding assays at equilibrium: Validation and interpretation. *Br. J. Pharmacol.* 2010; **161**, 1219-37.

[45] I Aier, PK Varadwaj and U Raj. Structural insights into conformational stability of both wild-type and mutant EZH2 receptor. *Sci. Rep.* 2016; **6**, 34984.

[46] KS Chopdar, GC Dash, PK Mohapatra, B Nayak and MK Raval. Monte-carlo method-based QSAR model to discover phytochemical urease inhibitors using SMILES and GRAPH descriptors. *J. Biomol. Struct. Dyn.* 2022; **40**, 5090-9.

[47] J Zhu, Y Lv, X Han, D Xu and W Han. Understanding the differences of the ligand binding/unbinding pathways between phosphorylated and non-phosphorylated ARH1 using molecular dynamics simulations. *Sci. Rep.* 2017; **7**, 12439.

[48] C Scott and S Griffin. Viroporins: Structure, function and potential as antiviral targets. *J. Gen. Virol.* 2015; **96**, 2000-27.

[49] J Kalikka and J Akola. Steered molecular dynamics simulations of ligand-receptor interaction in lipocalins. *Eur. Biophys. J.* 2011; **40**, 181-94.

[50] C Schmidt, JA Macpherson, AM Lau, KW Tan, F Fraternali and A Politis. Surface accessibility and dynamics of macromolecular assemblies probed by covalent labeling mass spectrometry and integrative modeling. *Anal. Chem.* 2017; **89**, 1459-68.

[51] JA Marsh and SA Teichmann. Relative solvent accessible surface area predicts protein conformational changes upon binding. *Structure* 2011; **19**, 859-67.

[52] M Candotti, A Pérez, C Ferrer-Costa, M Rueda, T Meyer, JL Gelpí and M Orozco. Exploring early stages of the chemical unfolding of proteins at the proteome scale. *Plos Comput. Biol.* 2013; **9**, e1003393.

[53] M Tarek and DJ Tobias. The role of protein-solvent hydrogen bond dynamics in the structural relaxation of a protein in glycerol versus water. *Eur. Biophys. J.* 2008; **37**, 701-9.

[54] D Zhang and R Lazim. Application of conventional molecular dynamics simulation in evaluating the stability of apomyoglobin in urea solution. *Sci. Rep.* 2017; **7**, 44651.

[55] P Nagy. Competing intramolecular vs. intermolecular hydrogen bonds in solution. *Int. J. Mol. Sci.* 2014; **15**, 19562-633.

[56] M Petukhov, G Rychkov, L Firsov and L Serrano. H-bonding in protein hydration revisited. *Protein Sci.* 2004; **13**, 2120-9.

[57] SNH Ishak, SNAM Aris, KBA Halim, MSM Ali, TC Leow, NHA Kamarudin, M Masomian and RNZRA Rahman. Molecular dynamic simulation of space and earth-grown crystal structures of thermostable T1 lipase geobacillus zalihae revealed a better structure. *Molecules* 2017; **22**, 1574.

[58] I Chikalov, P Yao, M Moshkov and JC Latombe. Learning probabilistic models of hydrogen bond stability from molecular dynamics simulation trajectories. *BMC Bioinformatics* 2011; **12**, S34.

[59] JL England and G Haran. Role of solvation effects in protein denaturation: From thermodynamics to single molecules and back. *Ann. Rev. Phys. Chem.* 2011; **62**, 257-77.

[60] RPP Valente, RC Souza, MG Medeiros, JEV Ferreira, RM Miranda, AHL Lima and JLSGV Junior. Using accelerated molecular dynamics simulation to elucidate the effects of the T198F mutation on the molecular flexibility of the West Nile virus envelope protein. *Sci. Rep.* 2020; **10**, 9625.

[61] M Batool, M Shah, MC Patra, D Yesudhas and S Choi. Structural insights into the Middle East respiratory syndrome coronavirus 4a protein and its dsRNA binding mechanism. *Sci. Rep.* 2017; **7**, 11362.

[62] U Doshi, MJ Holliday, EZ Eisenmesser and D Hamelberg. Dynamical network of residue-residue contacts reveals coupled allosteric effects in recognition, catalysis, and mutation. *Proc. Natl. Acad. Sci.* 2016; **113**, 4735-40.

[63] K Kasahara, I Fukuda and H Nakamura. A novel approach of dynamic cross correlation analysis on molecular dynamics simulations and its application to Ets1 Dimer-DNA complex. *PLoS One* 2014; **9**, e112419.

[64] D Ni, K Song, J Zhang and S Lu. Molecular dynamics simulations and dynamic network analysis reveal the allosteric unbinding of monobody to H-Ras triggered by R135K mutation. *Int. J. Mol. Sci.* 2017; **18**, 2249.